Published in final edited form as:
Biomaterials. 2012 August ; 33(22): 5524–5533. doi:10.1016/j.biomaterials.2012.04.017.

The effect of source animal age upon the *in vivo* remodeling characteristics of an extracellular matrix scaffold

Brian M. Sicari[a,c], **Scott A. Johnson**[a,b], **Bernard F. Siu**[a], **Peter M. Crapo**[a,b], **Kerry A. Daly**[a,b], **Hongbin Jiang**[a,b], **Christopher J. Medberry**[a], **Stephen Tottey**[a], **Neill J. Turner**[a,b], and **Stephen F. Badylak**[a,b,*]

[a]McGowan Institute for Regenerative Medicine, University of Pittsburgh, Pittsburgh, PA, USA

[b]Department of Surgery, University of Pittsburgh, Pittsburgh, PA, USA

[c]Department of Pathology, University of Pittsburgh, Pittsburgh, PA, USA

Abstract

Biologic scaffolds composed of mammalian extracellular matrix (ECM) are routinely used for the repair and reconstruction of injured or missing tissues in a variety of pre-clinical and clinical applications. However, the structural and functional outcomes have varied considerably. An important variable of xenogeneic biologic scaffolds is the age of the animal from which the ECM is derived. The present study compared the *in vivo* host response and remodeling outcomes of biologic scaffolds composed of small intestinal submucosa (SIS)-ECM harvested from pigs that differed only in age. Results showed that there are distinct differences in the remodeling characteristics as a consequence of source animal age. Scaffolds derived from younger animals were associated with a more constructive, site appropriate, tissue remodeling response than scaffolds derived from older animals. Furthermore, the constructive remodeling response was associated with a dominant M2 macrophage response.

Keywords

Age/ageing; ECM (extracellular matrix); Scaffold; Macrophage; Immune response; Mechanical properties

1. Introduction

Biologic scaffolds composed of xenogeneic extracellular matrix (ECM) are derived by the decellularization of mammalian tissues and have been used in both pre-clinical and clinical settings for the reconstruction of damaged or missing tissues [1–3]. ECM scaffolds can alter the default wound healing response from the well described pro-inflammatory and scarring events toward a more constructive remodeling response, i.e., the site appropriate formation of functional tissue, in a variety of anatomic locations including dermis [4], esophagus [5,6], skeletal muscle [3,7,8], and heart [10–12], among others. Results of such clinical applications have varied considerably [1,13–18], and the variables, which affect outcome, are only partially understood. Two intuitively important determinants of the remodeling outcome are the physical and biologic properties of the ECM scaffold material itself, and the innate immune response of the recipient. Modulation of macrophage phenotype, a critical

*Corresponding author. McGowan Institute for Regenerative Medicine, Bridge-side Point 2 Building, University of Pittsburgh, 450 Technology Drive, Suite 300, Pittsburgh, PA 15213, USA. Tel.: +1 412 624 5253; fax: +1 412 624 5256. badylaks@upmc.edu (S.F. Badylak).

component of the innate immune response, has been shown to play a prominent role in the scaffold remodeling outcome [19,20], but the effect of the age of tissue from which the ECM scaffold is prepared has been largely ignored.

Mammalian fetal wound healing is characterized by site- and tissue-specific regeneration and minimal scar tissue formation; a distinct contrast to wound healing in adults [21]. This tissue regeneration response is associated with selected pro-inflammatory events [22,23], increased capacity for wound closure [24,25], and a distinct ECM composition [26–29]. The ECM present in fetal tissues is enriched in glycosaminoglycans, which facilitate the proliferation and migration of a number of cell types [26,30,31]. The collagen content of fetal ECM is less mature and contains fewer cross-links when compared to adult ECM [32]. Minimal collagen cross-linking facilitates rapid ECM turnover and remodeling. Because of these characteristics, it is plausible that biologic materials derived from neonatal or newborn tissues may be better suited as inductive scaffolds than biologic scaffold materials derived from older animals.

The diverse remodeling outcomes associated with ECM scaffold use can also be attributed to variables such as processing methods [8], source species and tissue origin of the ECM [33], post implantation mechanical load [34], and decellularization efficiency [35]. Because the response to tissue injury is known to be more favorable and robust in young vs. aged mammals, some biologic scaffolds use source materials that include ECM derived from fetal cells or mammals [36,37]. It has been previously reported that distinct differences exist in the mechanical, structural, and *in vitro* biologic properties of ECM harvested from different aged animals (summarized in Table 1) [38]. However, the effect of donor animal age upon the *in vivo* remodeling characteristics of xenogeneic ECM scaffolds has not been systematically examined.

The objective of the present study was to compare the *in vivo* remodeling outcome of ECM scaffolds that differ only in source animal age. An established rodent model of abdominal wall muscle reconstruction was used [39] to evaluate the host remodeling response, including the phenotype of responding macrophages, scaffold induced vascularity, innervation, and myogenesis over time, and the mechanical properties of the remodeled injury site after 26-weeks.

2. Materials and methods

2.1. Overview of experimental design

Small intestinal submucosa (SIS)-ECM was prepared from the small intestine of 4 distinctly different aged pigs of identical gene pool and husbandry: 3-weeks, 12-weeks, 26-weeks, and greater than 52-weeks of age. The different aged tissues were collected, decellularized, and processed at the same time using identical methods and the resulting SIS-ECM was used to repair a 1.0 cm by 1.0 cm partial thickness abdominal wall musculature defect in a Sprague–Dawley rat model. Treatment groups were equally and randomly subdivided and sacrificed at 14, 28, 120, or 180 days post-surgery. Following euthanasia and explantation of the remodeled scaffold materials, mechanical testing and histologic and immunolabeling methods were used to determine the mechanical and morphologic characteristics of the remodeled tissue (Table 2).

2.2. Source and preparation of ECM material

The jejunum from Whiteshire Hamroc pigs of 4 distinctly different ages (3,12, 26 and >52-weeks) were harvested immediately following euthanasia (Tissue Source, Lafayette, IN). The animals were of identical genetic heritage, and were raised and kept in identical husbandry conditions including diet and vaccination history. All tissues were harvested on

the same day and stored on ice prior to processing to create SIS-ECM as previously described [40,41]. Briefly, the intestines were rinsed with water and the mesenteric tissues were removed. The intestines were cut longitudinally and mechanically delaminated to remove the tunica serosa, tunica muscularis externa, and the luminal portion of the tunica mucosa including most of the lamina propria. After delamination, the tunica submucosa and the basilar layer of the tunica mucosa including the muscularis mucosa and the stratum compactum of the lamina propria remained. The material was further decellularized using 0.1% (v/v) peracetic acid (Rochester Midland Corporation, Rochester, NY) followed by multiple rinses with saline and deionized water. The SIS-ECM material was then vacuum pressed to form 4-layer constructs and cut to 1 cm^2 in size before being terminally sterilized with ethylene oxide.

2.3. Surgical procedure

All procedures were performed in accordance with the National Institute of Health (NIH) guidelines for care and use of laboratory animals, and with approval of the Institutional Animal Care and Use Committee (IACUC) at the University of Pittsburgh. Adult female Sprague–Dawley rats weighing approximately 300 g (Charles River Laboratory, Wilmington MA) were subjected to partial thickness abdominal wall defect surgery [19,42]. Animals were separated into groups based on treatment type: (1) uninjured control, (2) untreated defect, (3) autologous tissue graft, (4) scaffold from >52-week-old source, (5) scaffold from 26-week-old source, (6) scaffold from 12-week-old source, (7) scaffold from 3-week-old source; and harvest time point: 14, 28, 120 and 180 days ($n = 3$ body walls per treatment group at 14, 28, and 120 days; $n = 8$ body walls per treatment group at 180 days; 119 total surgeries were performed). Five implant sites per treatment group were used for mechanical testing at 180 days only, and three implant sites per treatment group were used for histologic analysis at each time point.

Each animal was anesthetized with 2% isoflurane in oxygen and the ventral abdomen was prepared by hair clipping and scrubbing with Betadine (povidone-iodine) before the placement of sterile drapes around the surgical site. A ventral midline abdominal skin incision was created. The subcutaneous tissues were bluntly dissected from the underlying muscle tissues on one side of the midline for a distance of approximately 4 cm to the anterior axillary line exposing the oblique musculature. A 1.0 cm^2 partial thickness defect consisting of the internal and external oblique layers of the abdominal wall musculature was excised while leaving the underlying transversalis fascia and peritoneum intact. The defect was left untreated or repaired with a 1.0 cm^2 piece of the chosen test article. A single 4-0 prolene suture was placed at each of the four corners of the test article to secure it to the adjacent abdominal wall musculature, allowing it to be exposed to a physiologic mechanical load and identifying the boundary of the implant at the time of necropsy. Interrupted subcuticular 4-0 Vicryl suture was used for skin closure. Each animal was allowed to recover from anesthesia on a heating pad and was returned to the housing unit.

Each animal received 0.06 mg Buprenex (buprenorphine hydrochloride) by subcutaneous injection the day of surgery and for two additional days. Baytril (5 mg) was given orally the day of surgery and for two additional days. The dietary habits, general health status, and the surgical site were monitored daily and recorded.

2.4. Euthanasia and specimen harvest

Animals were sacrificed at 14, 28, 120, or 180 days. Each rat was euthanized with 5% isoflurane in oxygen followed by an intracardiac injection of 5 mL of potassium chloride to induce cardiac arrest. Implants for histologic evaluation ($n = 3$), including ~2 mm of surrounding native abdominal wall musculature, was excised, mounted on corkboard to

maintain *in situ* size and shape, and placed in 10% neutral buffered formalin. Implants for mechanical testing ($n = 5$) were placed in Ringer's solution immediately after excision for uniaxial tensile testing.

2.5. Histologic and immunolabeling analysis

The tissue was embedded in paraffin, cut into 5-um thick sections, and mounted onto glass slides before being stained with Masson's Trichome or Movat's Pentachrome. The primary antibodies used for the immunolabeling studies were: (1) monoclonal anti-myosin (skeletal, slow, clone NOQ7.5.4D; Sigma Aldrich, St. Louis, MO) at 1:4000 dilution for identification of slow (type I) skeletal muscle fibers; (2) monoclonal anti-myosin (skeletal, fast, alkaline phosphatase conjugate, clone MY-32, Sigma Aldrich) at 1:200 dilution for identification of fast (type II) skeletal muscle fibers; (3) rabbit polyclonal CD31 (Abcam, Cambridge, MA) at 1:100 dilution for identification of endothelial cells; (4) anti-Beta-III Tubulin (Dako USA, Carpinteria, CA) at 1:200 dilution for identification of neurons; (5) goat polyclonal CD206 (Santa Cruz Biotech, Santa Cruz, CA) at 1:100 for identification of M2 macrophages; (6) rabbit monoclonal CCR7 (Epitomics, Burlingame, CA) at 1:100 for identification of M1 macrophages; and (7) mouse-anti rat CD68 (Serotec, Raleigh, NC) at 1:50, as a pan macrophage marker. Table 2 shows the details of the specific staining performed at each time point.

To identify fast and slow muscle fibers, unstained sections were de-paraffinized and heat-mediated epitope retrieval was performed with 0.1 mM EDTA buffer at 95–100 °C for 25 min followed by enzyme-mediated antigen retrieval with 0.1% (v/v) trypsin/0.1% (w/v) calcium chloride digestion at 37 °C for 10 min. Slides were washed in Tris buffered saline (TBS), pH 7.6, then incubated for 10 min in a blocking solution containing 0.1% (v/v) Tween 20, 0.1% (v/v) Triton X, 2% (v/v) normal horse serum and 2% (v/v) normal goat serum at room temperature to prevent non-specific antibody binding. To inhibit endogenous peroxidase activity, the slides were incubated with 3% (v/v) hydrogen peroxide (Spectrum, New Brunswick, NJ) in methanol for 10 min at room temperature. The slow anti-myosin antibody was applied and incubated for 30 min at room temperature. The slides were then incubated with the secondary antibody (biotinylated anti-rabbit; Vector) at 1:200 for 30 min at room temperature, followed by horseradish peroxidase solution (Vector) for 30 min at 37°C. Diaminobenzidine (DAB) (Vector) was applied to detect positive staining cells. The blocking solution was then applied again for 10 min at room temperature, followed by the fast anti-myosin antibody for 60 min at room temperature. Red alkaline phosphatase substrate was applied to detect positive staining (Vector).

For Beta-III Tubulin immunolabeling, slides were de-paraffinized, and heat-mediated epitope retrieval was performed as described above. The slides were washed in phosphate buffered saline (PBS) then incubated for 30 min with 2% (v/v) normal horse serum (Vector) at 37 °C to prevent non-specific antibody binding. Endogenous peroxidase activity was inhibited by incubating with 3% (v/v) hydrogen peroxide (Spectrum) in methanol for 30 min at room temperature. The tissue sections were then incubated in the Beta-III Tubulin primary antibody for 1 h at room temperature, followed by the secondary antibody (biotinylated anti-mouse; Vector) at 1:200 for 30 min at room temperature. Horseradish peroxidase solution (Vector) was applied for 30 min at 37 °C, and diaminobenzidine (DAB) (Vector) was used to detect positive staining cells. The slides were counterstained with hematoxylin.

Similarly, for CD31 immunolabeling the slides were de-paraffinized and heat-mediated epitope retrieval was performed with 0.01 M citrate buffer (Spectrum), pH 6.0, at 95–100 °C for 20 min. Enzyme-mediated antigen retrieval was then performed using proteinase K in a buffer of 50 mM Tris base and 1 mM EDTA, pH 8.0, at 60 °C for 10 min. Following washes

in PBS, the slides were incubated for 60 min with 2% normal horse serum (Vector) at 37 °C to prevent non-specific antibody binding, followed by a 30 min incubation in 3% (v/v) hydrogen peroxide. The tissue sections were then incubated in the CD31 primary antibody for 1 h at room temperature, followed by the secondary antibody for 30 min at 37 °C. Horseradish peroxidase solution (Vector) was applied for 30 min at 37 °C. Diaminobenzidine (DAB) (Vector) was used to detect positive staining cells and the slides were counterstained with hematoxylin.

M1 vs. M2 polarized macrophages were identified by immunolabeling. After de-paraffinization, heat-mediated antigen retrieval was performed with 0.01 M citrate buffer (Spectrum), pH 6.0, at 95–100 °C for 20 min. Tissue sections were incubated in blocking buffer (1% (w/v) bovine serum albumin/0.05% (v/v) Tween-20/0.05% Triton X-100 (v/v)) for 1 h. The primary antibodies (CD206, CCR7, and CD68), diluted in blocking buffer, were then added to the slides for 16 h at 4 °C in a humidified chamber. The secondary antibodies (also diluted in blocking buffer) were incubated on the slides for 1 h in a humidified chamber at room temperature. The secondary antibodies used were Alexa Fluor® goat anti-rabbit 568 (Invitrogen), Alexa Fluor® donkey anti-goat 488 (Invitrogen) and Alexa Fluor® donkey anti-mouse 350 (Invitrogen). Draq5 (Cell Signaling Technologies, Danvers MA) was used as a nuclear counterstain.

2.6. Image analysis

All tissue sections were imaged using a Zeiss Axio Observer Z1 or Nikon E600 microscope with Nuance multispectral imaging system (CRI Inc, Cambridge MA) with appropriate brightfield and fluorescent filter sets. Three random Masson stained images of the device implant site at the interface with native tissue were taken at 100× magnification. A quantitative analysis of the trichrome staining was conducted by determining the percent of blue stained tissue within the surgical site using the Nuance software. Collagen or connective tissue (blue) and nuclei or muscle fibers (red) were isolated by spectral filtration and subsequent thresholding. High percent blue staining indicates the predominant presence of collagenous connective tissue.

Quantification of M1/M2 polarization was achieved using a custom image analysis pipeline developed using the cell profiler image analysis package [43,44]. This custom pipeline identified and quantified the number of CD68 + CCR7+ (M1 macrophage phenotype) and CD68 + CD206 + (M2 macrophage phenotype) cells present within scaffold implantation sites. Any cells that co-expressed the CCR7 and CD206 markers were excluded. These values were then expressed as a ratio of M1:M2.

Quantification of CD31 positive blood vessels was done by immunolabeling and counting the number of blood vessels per 400× field of view (FOV). Six images of each surgical site where quantified by two blinded independent investigators. Only positively labeled cells that were associated with a visible lumen were counted.

Quantification of fast vs. slow myofibers was done by immunolabeling and counting the number of fast (red) and slow (brown) muscle fibers per 200× FOV. Three images of each surgical site where quantified.

2.7. Mechanical testing

Tissue explants were trimmed to dog-bone geometry (midsubstance width 5.7 ± 1.6 mm, length 20.4 ± 6.6 mm) with exact specimen dimensions dependent on animal and explant size. All specimens were subjected to 10 pre-load cycles (25.4 mm/min, 0.1–0.5 N) immediately prior to testing to failure (25.4 mm/min). Ultimate tensile stress was calculated from the peak load, width, and thickness (2.3 ± 0.5 mm): $\sigma = F/(w*t)$. Strain at failure was

calculated by dividing the change in length by the original length: $\varepsilon = \Delta L/L_O$. Elastic modulus was taken as the slope of the stress-strain curve in the range of 20–60% of the ultimate tensile stress: $E = 0.4*\sigma/(\varepsilon_{60\%\sigma} - \varepsilon_{20\%\sigma})$. Five specimens were tested from each control and experimental group with the following exceptions: native tissue = 9; SIS-ECM implant from >52-week aged source = 4.

2.8. Statistical analysis

A one-way analysis of variance (ANOVA) was used in conjunction with a Turkey's post-hoc test to compare results between groups. Differences were considered significant at $p < 0.05$. Statistical analysis was completed using SPSS Statistical Analysis Software (IBM, Chicago, IL, USA). All error bars represent standard deviations.

3. Results

3.1. Histomorphologic and immunolabeling findings

All treatment groups elicited a robust cellular infiltrate consisting mostly of mononuclear cells after 14 days (Fig. 1A). Angiogenesis was also observed in all groups at day 14 and remained a feature of the remodeling process throughout the entire study (Fig. S1). All of the ECM scaffold materials degraded completely based upon morphologic analysis and were replaced with host tissue by 180 days. No GAG's or elastins were observable within the remodeling surgical sites for the duration of the study (Fig. S2). However, there were notable differences in the remodeling responses to the different aged ECM materials, which are detailed below.

3.1.1. Untreated defect—Untreated defect sites were characterized by a loose collagenous connective tissue after 14 days. A mononuclear cell infiltrate was localized to the defect margins (Fig. 1A). Immunolabeling studies showed an M1:M2 macrophage ratio of 1.24 ± 0.21 indicating a predominant M1 macrophage response (Fig. 1B, C). After 180 days untreated defects formed dense collagenous tissue consistent with scar tissue (Fig. 2). Quantitative analysis of the trichrome staining over time showed an increase in the amount of collagenous connective tissue within the defect site after 180 days when compared to the 14 day time point ($p < 0.005$) (Fig. 3). After 180 days the defect site showed no evidence of new skeletal muscle or nerve (Figs. 4 and 5).

3.1.2. Autologous tissue graft—Treatment of the defect site with autologous tissue elicited a mononuclear infiltrate that was localized around the remnants of necrotic skeletal muscle within the autograft after 14 days. Similar to untreated defects, immunolabeling studies showed an M1:M2 macrophage ratio of 1.27 ± 0.24 indicating a predominant M1 macrophage response (Fig. 1B, C). Between 28 and 120 days there was a decreased cellular infiltrate and loss of skeletal muscle within the autograft although small islands of necrotic skeletal muscle could still be identified (Fig. S3). After 180 days the autologous tissue graft had remodeled into dense and relatively acellular collagenous tissue (Fig. 2). The surgical site showed no evidence of new skeletal muscle tissue (Fig. 4) or signs of innervation (Fig. 5). Quantitative analysis of the Masson's trichrome staining over time revealed an increase in the amount of collagenous connective tissue at 180 days when compared to the 14 ($p < 0.01$) and 28 ($p < 0.09$) day time points (Fig. 3).

3.1.3. SIS-ECM graft from 3-week-old animals—The SIS-ECM graft from 3-week-old source showed a mono-nuclear cell infiltrate throughout the entire scaffold at 14 days (Fig. 1A). Small remnants of the original ECM implant and a large amount of host derived neomatrix were present within the defect site. Immunolabeling studies showed an M1:M2 macrophage ratio of 0.67 ± 0.13 indicating a predominant M2 macrophage response after 14

days. At 28 days SIS-ECM scaffolds from 3-week-old source showed a decreased cellularity and were replaced with host derived matrix (Fig. S3). Small islands of skeletal muscle could be seen scattered throughout the defect site after 120 days. At 180 days the implant site contained new host tissue that contained organized bundles of new skeletal muscle myofibers surrounded by partially organized collagenous connective tissue (Fig. 2). In addition, like native tissue and SIS-ECM from 12-week-old source treated defects described below, the majority of the muscle fibers within the defect site stained positive for fast type II myosin with slow type I myosin fibers dispersed throughout the remodeled scaffold placement site (Fig. 4A). Furthermore, the 12-week-old scaffold showed an increase in the presence of slow myosin muscle fibers when compared to all other interventions. Nerve fibers were present adjacent to the myofibers throughout the defect site (Fig. 5). Quantitative analysis of the Masson's trichrome stained 3-week-old source SIS-ECM treated defects showed an increase in collagenous connective tissue between 14 and 120 days ($p < 0.018$) (Fig. 3). The surgical site further remodeled and became partially replaced with skeletal muscle tissue, resulting in a decreased collagen percentage at 180 days when compared to the 120 day time point ($p < 0.03$). This collagen percentage at 180 days was not significantly different from that at 14 days (Fig. 3).

3.1.4. SIS-ECM graft from 12-week-old animals—The SIS-ECM graft from 12-week-old source treated defect sites showed a mononuclear cell infiltrate throughout the scaffold at 14 days (Fig. 1A). In addition at 14 days, small remnants of the original ECM implant were present within the defect site. Immunolabeling studies showed an M1:M2 macrophage ratio of 0.69 ± 0.11 indicating a predominant M2 macrophage response. After 28 days the SIS-ECM grafts showed decreased cellularity and at 120 days small islands of skeletal muscle were present (Fig. S3). SIS-ECM scaffolds from 12-week-old source remodeled in a similar fashion to that of the 3-week-old source. At 180 days the implant site contained new host tissue that consisted of organized bundles of skeletal muscle myofibers surrounded by partially organized collagenous connective tissue (Fig. 2). Similar to native tissue, the majority of the muscle fibers within the defect site stained positive for fast type II myosin with a smaller number of widely dispersed slow type I myosin fibers (Fig. 4A and B). Nerve fibers were present adjacent to the myofibers throughout the defect site (Fig. 5). Quantitative analysis of the Masson's trichrome stained treated defect site tissues showed a slight increase in collagenous connective tissue between 14 and 120 days ($p < 0.001$) (Fig. 3). The surgical site further remodeled and became partially replaced with skeletal muscle tissue, resulting in a decreased collagen percentage at 180 days when compared to the 120 day time point ($p < 0.004$). This collagen percentage at 180 days was not significantly different from that at 14 days (Fig. 3).

3.1.5. SIS-ECM graft from 26-week-old animals—The SIS-ECM graft from 26-week-old source treated defect sites showed a mononuclear cell infiltrate throughout the scaffold at 14 days (Fig. 1A). Original ECM scaffold material could be identified along with host derived neomatrix. Immunolabeling studies showed an M1:M2 macrophage ratio of 0.95 ± 0.24 indicating a balanced macrophage phenotype response (Fig. 1B, C). At 28 days the surgical site showed a decreased cellularity and increased amount of neomatrix. At 120 days no evidence of the original implanted scaffold was observed and small islands of skeletal muscle could be identified within the defect site (Fig. S3). At 180 days isolated skeletal muscle myofibers were dispersed between collagenous connective tissue throughout the defect site (Fig. 2). These individual myofibers stained positive for fast type II myosin (Fig. 4A and B) and were adjacent to nerve fibers (Fig. 5). Quantitative analysis of the Masson's trichrome staining over time revealed an increase in the amount of collagenous connective tissue at 180 days when compared to the 14 ($p < 0.001$) and 28 ($p < 0.046$) day time points (Fig. 3).

3.1.6. SIS-ECM graft from >52-week-old animals—The SIS-ECM graft from >52-week-old source treated defect sites elicited a cellular infiltrate which was localized around the suture lines and did not completely penetrate the full thickness of the scaffold at 14 days (Fig. 1A). In addition at 14 days, much of the original ECM scaffold could be identified along with a small amount of host derived neomatix. Immunolabeling studies showed an M1:M2 macrophage ratio of 0.93 ± 0.18 indicating a balanced macrophage phenotype response (Fig. 1B, C). After 28 and 120 days the >52-week-old source SIS-ECM treated defects showed decreased cellularity with remnants of the ECM implant (Fig. S3). At 180 days the >52-week-old source SIS-ECM treated defect sites contained pockets of cellularity surrounded by collagenous connective tissue (Fig. 2). No evidence of the originally implanted scaffold was observed and there were no signs of new skeletal muscle or innervation (Figs. 4 and 5). Quantitative analysis of the Masson's trichrome staining over time revealed an increase in the amount of collagenous connective tissue at 180 days when compared to the 14 ($p < 0.001$) and 28 ($p < 0.001$) day time points (Fig. 3).

3.2. Mechanical testing

Rat abdominal body wall containing remodeled SIS-ECM grafts from 3-week-old source withstood greater uniaxial tensile stress compared to all other control and experimental groups as determined by ANOVA and Tukey–Kramer post-hoc evaluation (Fig. 6A). No other differences were found to be significant. Strain at failure and modulus did not differ significantly for control and experimental groups, including native body wall, body wall with a defect site that remained untreated, body wall treated with autologous tissue, or body wall treated with SIS-ECM from 3, 12, 26, and >52-week-old animals (Fig. 6B–C).

4. Discussion

The present study represents a systematic comparison of the *in vivo* host response to xenogeneic biologic scaffold materials that differ by a single variable; specifically, age of the animal from which the source tissue was harvested. There are two outcomes of note. First, source animal age is an important variable and ECM harvested from 3-week-old and 12-week-old pigs promotes the formation of greater amounts of site appropriate skeletal muscle tissue than ECM harvested from older pigs. Secondly, the constructive site appropriate remodeling response is associated with a predominant M2 macrophage response.

It is well known that fetal and neonatal mammals have greater wound healing and regenerative potential than adult mammals. The composition of fetal and neonatal ECM is distinctly different from that of adults and plays an important role in tissue development [45,46]. Fetal wounds have increased amounts of glycosaminoglycans (GAGs) such as hyaluronic acid and chondroitin sulfate [26,29], which facilitate cell migration, mitosis, and differentiation [30]. Compared to ECM in mature mammals, the ECM of fetal tissue is composed of more immature collagen containing fewer molecular cross-links; a feature which promotes rapid degradation and remodeling [32]. Therefore it is logical and plausible that bioscaffolds composed of ECM derived from fetal or neonatal tissues would induce a more robust and constructive tissue remodeling response than ECM derived from adult tissues. The results of the present study are consistent with this hypothesis.

The mechanisms by which scaffolds composed of ECM mediate a favorable remodeling process are not fully understood but include ECM scaffold degradation with the generation of bioactive cryptic peptides [47] release of bound growth factors [48], recruitment of endogenous stem and progenitor cells [49,50], and modulation of the innate immune response [19,20], among others. Of these potential mechanisms, only a component of the innate immune response was investigated in the present study; specifically, macrophage phenotype. A previous study compared the *in vitro* structural, mechanical, compositional,

and bioactive properties of the same differently aged SIS-ECM materials [38]. Scaffolds composed of 3-week-old and 12-week-old source ECM elicited increased progenitor cell chemotaxis and showed greater glycosaminoglycan (GAG) content than ECM scaffolds derived from older tissues (Table 1). Given the differences we have identified in the composition of differently aged ECMs it is plausible or logical that the decellularization protocol affected the ECMs in different ways. Such phenomena may in part explain the differences in remodeling outcome. The purpose of the present study was not to determine cause-effect relationships between the variables from the previous study (Table 1), but rather to determine the association of source tissue age within downstream remodeling events in an animal model of body wall reconstruction.

The response of skeletal muscle, which is a prominent natural component of the abdominal body wall, to injury is dependent on the temporal participation of different macrophage phenotypes [51]. These macrophage phenotypes are characterized by distinct functional properties, effector molecule production, and surface marker expression [52,53]. Macrophage phenotypes range from classically activated (M1) macrophages which are pro-inflammatory at one end of a spectrum to alternatively activated (M2) macrophages which facilitate constructive tissue remodeling and repair at the opposite end of the spectrum [53,54]. Following an initial M1 macrophage response, which stimulates muscle progenitor cell recruitment and mitosis, a subsequent predominant M2 macrophage response promotes the differentiation of skeletal muscle precursor cells [51]. Inhibition of the M2 phenotype results in a severe lack of muscle regeneration and an accentuation of inflammation and necrosis [55]. Dominant M1 or M2 macrophage populations at the *in situ* interface of host tissue with ECM scaffolds are associated with either chronic inflammation with fibrotic tissue deposition or site appropriate tissue restoration, respectively [56] In the present study, scaffolds derived from younger animals were associated with a predominant M2 macrophage response after 14 days and showed the greatest amount of skeletal muscle at 180 days; a finding consistent with the predictive association of the M2 phenotype with favorable remodeling of surgical mesh products composed of biologic materials. It has previously been shown that surgically implanted ECM scaffolds enhance a host M2 macrophage response [19]. The specific cause of the robust M2 response found within ECM scaffolds manufactured from 3-week-old or 12-week-old pig tissues are unknown.

Repair of rat abdominal body wall with SIS-ECM from distinctly different aged animals resulted in remodeled tissue with similar mechanical properties to those of native body wall (Fig. 6). However, SIS-ECM from 3-week-old animals remodeled into stronger tissue compared to native body wall (Fig. 6A). Based on a previous study [38], it is likely that biologic cues from degradation products of 3-week-old source SIS-ECM vary from those of degrading SIS-ECM from older animals and lead to different downstream remodeling outcomes. It is possible that because the 3-week-old source scaffolds degraded more rapidly and promoted greater cell migration [38], the skeletal muscle tissue that formed within the 3-week-old source SIS-ECM treated surgical sites had more time to mature, and this in combination with the increased amount of connective tissue, compared to native tissue, resulted in stronger tissue. In addition, passive mechanical testing may not have been sensitive enough to detect discernible differences in such a small defect site. Furthermore, biologic variability between animals may also have masked subtle differences between experimental groups. However, mechanical data in this study clearly showed that donor age could impact functional outcomes.

The present study compared xenogeneic biologic scaffold materials differing only in source animal age. However, there are limitations that must be noted in the interpretation of the data. First, the results represent the findings from a single source tissue of ECM material; specifically porcine SIS-ECM. These results cannot necessarily be generalized to ECM

prepared from other tissue sources such as dermis, urinary bladder, and others. Secondly, ECM materials are prepared by decellularization of various tissues, and the decellularization procedures utilized can vary significantly. Results of the present study may not apply to materials prepared by other methods that affect surface epitopes, biochemical composition, and rate of degradation of various scaffold materials. Finally, the association of the M1/M2 macrophage phenotype ratio with constructive remodeling does not prove cause-effect.

5. Conclusions

The present study examines an important variable that should be considered in the design and manufacturing of biologic devices composed of mammalian ECM; specifically, the age of the source animal. Biologic scaffold materials derived from younger (3 and 12-week-old) aged animals are associated with a host innate immune response consisting predominantly of M2 macrophages and a more robust constructive remodeling response when compared to scaffolds prepared from 26-week-old or >52-week-old pigs. The specific physical and/or biologic factors responsible for the different remodeling outcomes are worthy of future investigations.

Supplementary Material

Refer to Web version on PubMed Central for supplementary material.

References

1. Badylak SF, Hoppo T, Nieponice A, Gilbert TW, Davison JM, Jobe BA. Esophageal preservation in five male patients after endoscopic inner-layer circumferential resection in the setting of superficial cancer: a regenerative medicine approach with a biologic scaffold. Tissue Eng Part A. 2011; 17(11–12):1643–50. [PubMed: 21306292]
2. Mase VJ Jr, Hsu JR, Wolf SE, Wenke JC, Baer DG, Owens J, et al. Clinical application of an acellular biologic scaffold for surgical repair of a large, traumatic quadriceps femoris muscle defect. Orthopedics. 2010; 33(7):511. [PubMed: 20608620]
3. Turner NJ, Yates AJ Jr, Weber DJ, Qureshi IR, Stolz DB, Gilbert TW, et al. Xenogeneic extracellular matrix as an inductive scaffold for regeneration of a functioning musculotendinous junction. Tissue Eng Part A. 2010; 16(11):3309–17. [PubMed: 20528669]
4. Brigido SA, Boc SF, Lopez RC. Effective management of major lower extremity wounds using an acellular regenerative tissue matrix: a pilot study. Orthopedics. 2004; 27(1 Suppl):s145–9. [PubMed: 14763548]
5. Nieponice A, McGrath K, Qureshi I, Beckman EJ, Luketich JD, Gilbert TW, et al. An extracellular matrix scaffold for esophageal stricture prevention after circumferential EMR. Gastrointest Endosc. 2009; 69(2):289–96. [PubMed: 18657808]
6. Nieponice A, Gilbert TW, Badylak SF. Reinforcement of esophageal anastomoses with an extracellular matrix scaffold in a canine model. Ann Thorac Surg. 2006; 82(6):2050–8. [PubMed: 17126109]
7. De Deyne PG, Kladakis SM. Bioscaffolds in tissue engineering: a rationale for use in the reconstruction of musculoskeletal soft tissues. Clin Podiatr Med Surg. 2005; 22(4):521–32. v. [PubMed: 16213377]
8. Valentin JE, Turner NJ, Gilbert TW, Badylak SF. Functional skeletal muscle formation with a biologic scaffold. Biomaterials. 2010; 31(29):7475–84. [PubMed: 20638716]
10. Akhyari P, Kamiya H, Haverich A, Karck M, Lichtenberg A. Myocardial tissue engineering: the extracellular matrix. Eur J Cardiothorac Surg. 2008; 34(2):229–41. [PubMed: 18502661]
11. Kochupura PV, Azeloglu EU, Kelly DJ, Doronin SV, Badylak SF, Krukenkamp IB, et al. Tissue-engineered myocardial patch derived from extracellular matrix provides regional mechanical function. Circulation. 2005; 112(9 Suppl):I144–9. [PubMed: 16159807]

12. Badylak SF, Kochupura PV, Cohen IS, Doronin SV, Saltman AE, Gilbert TW, et al. The use of extracellular matrix as an inductive scaffold for the partial replacement of functional myocardium. Cell Transplant. 2006; 15(Suppl 1):S29–40. [PubMed: 16826793]
13. Ayyildiz A, Akgul KT, Huri E, Nuhoglu B, Kilicoglu B, Ustun H, et al. Use of porcine small intestinal submucosa in bladder augmentation in rabbit: long-term histological outcome. ANZ J Surg. 2008; 78(1–2):82–6. [PubMed: 18199213]
14. Zalavras CG, Gardocki R, Huang E, Stevanovic M, Hedman T, Tibone J. Reconstruction of large rotator cuff tendon defects with porcine small intestinal submucosa in an animal model. J Shoulder Elbow Surg. 2006; 15(2):224–31. [PubMed: 16517370]
15. Adams JE, Zobitz ME, Reach JS Jr, An KN, Steinmann SP. Rotator cuff repair using an acellular dermal matrix graft: an in vivo study in a canine model. Arthroscopy. 2006; 22(7):700–9. [PubMed: 16843804]
16. Zheng MH, Chen J, Kirilak Y, Willers C, Xu J, Wood D. Porcine small intestine submucosa (SIS) is not an acellular collagenous matrix and contains porcine DNA: possible implications in human implantation. J Biomed Mater Res B Appl Biomater. 2005; 73(1):61–7. [PubMed: 15736287]
17. Doede T, Bondartschuk M, Joerck C, Schulze E, Goernig M. Unsuccessful alloplastic esophageal replacement with porcine small intestinal submucosa. Artif Organs. 2009; 33(4):328–33. [PubMed: 19335409]
18. Walton JR, Bowman NK, Khatib Y, Linklater J, Murrell GA. Restore orthobiologic implant: not recommended for augmentation of rotator cuff repairs. J Bone Joint Surg Am. 2007; 89(4):786–91. [PubMed: 17403801]
19. Badylak SF, Valentin JE, Ravindra AK, McCabe GP, Stewart-Akers AM. Macrophage phenotype as a determinant of biologic scaffold remodeling. Tissue Eng Part A. 2008; 14(11):1835–42. [PubMed: 18950271]
20. Brown BN, Valentin JE, Stewart-Akers AM, McCabe GP, Badylak SF. Macrophage phenotype and remodeling outcomes in response to biologic scaffolds with and without a cellular component. Biomaterials. 2009; 30(8):1482–91. [PubMed: 19121538]
21. Rowlatt U. Intrauterine wound healing in a 20 week human fetus. Virchows Arch A Pathol Anat Histol. 1979; 381(3):353–61. [PubMed: 155931]
22. Cowin AJ, Brosnan MP, Holmes TM, Ferguson MW. Endogenous inflammatory response to dermal wound healing in the fetal and adult mouse. Dev Dyn. 1998; 212(3):385–93. [PubMed: 9671942]
23. Hopkinson-Woolley J, Hughes D, Gordon S, Martin P. Macrophage recruitment during limb development and wound healing in the embryonic and foetal mouse. J Cell Sci. 1994; 107(Pt 5): 1159–67. [PubMed: 7929625]
24. Brock J, Midwinter K, Lewis J, Martin P. Healing of incisional wounds in the embryonic chick wing bud: characterization of the actin purse-string and demonstration of a requirement for Rho activation. J Cell Biol. 1996; 135(4):1097–107. [PubMed: 8922389]
25. Martin P, Lewis J. Actin cables and epidermal movement in embryonic wound healing. Nature. 1992; 360(6400):179–83. [PubMed: 1436096]
26. Sawai T, Usui N, Sando K, Fukui Y, Kamata S, Okada A, et al. Hyaluronic acid of wound fluid in adult and fetal rabbits. J Pediatr Surg. 1997; 32(1):41–3. [PubMed: 9021565]
27. West DC, Shaw DM, Lorenz P, Adzick NS, Longaker MT. Fibrotic healing of adult and late gestation fetal wounds correlates with increased hyaluronidase activity and removal of hyaluronan. Int J Biochem Cell Biol. 1997; 29(1):201–10. [PubMed: 9076955]
28. Whitby DJ, Ferguson MW. The extracellular matrix of lip wounds in fetal, neonatal and adult mice. Development. 1991; 112(2):651–68. [PubMed: 1724421]
29. Longaker MT, Whitby DJ, Ferguson MW, Harrison MR, Crombleholme TM, Langer JC, et al. Studies in fetal wound healing: III early deposition of fibronectin distinguishes fetal from adult wound healing. J Pediatr Surg. 1989; 24(8):799–805. [PubMed: 2769549]
30. Toole BP, Wight TN, Tammi MI. Hyaluronan-cell interactions in cancer and vascular disease. J Biol Chem. 2002; 277(7):4593–6. [PubMed: 11717318]

31. Longaker MT, Chiu ES, Adzick NS, Stern M, Harrison MR, Stern R. Studies in fetal wound healing. V. A prolonged presence of hyaluronic acid characterizes fetal wound fluid. Ann Surg. 1991; 213(4):292–6. [PubMed: 2009010]
32. Lovvorn HN III, Cheung DT, Nimni ME, Perelman N, Estes JM, Adzick NS. Relative distribution and crosslinking of collagen distinguish fetal from adult sheep wound repair. J Pediatr Surg. 1999; 34(1):218–23. [PubMed: 10022176]
33. Badylak SF. The extracellular matrix as a biologic scaffold material. Biomaterials. 2007; 28(25): 3587–93. [PubMed: 17524477]
34. Boruch AV, Nieponice A, Qureshi IR, Gilbert TW, Badylak SF. Constructive remodeling of biologic scaffolds is dependent on early exposure to physiologic bladder filling in a canine partial cystectomy model. J Surg Res. 2010; 161(2):217–25. [PubMed: 19577253]
35. Keane TJ, Londono R, Turner NJ, Badylak SF. Consequences of ineffective decellularization of biologic scaffolds on the host response. Biomaterials. 2012; 33(6):1771–81. [PubMed: 22137126]
36. Eaglstein WH, Falanga V. Tissue engineering and the development of Apligraf a human skin equivalent. Adv Wound Care. 1998; 11(4 Suppl):1–8. [PubMed: 10326339]
37. Bhattacharya N. Fetal cell/tissue therapy in adult disease: a new horizon in regenerative medicine. Clin Exp Obstet Gynecol. 2004; 31(3):167–73. [PubMed: 15491058]
38. Tottey S, Johnson SA, Crapo PM, Reing JE, Zhang L, Jiang H, et al. The effect of source animal age upon extracellular matrix scaffold properties. Biomaterials. 2011; 32(1):128–36. [PubMed: 20870285]
39. Satheesha Nayak B, Rodenbaugh DW. Modeling the anatomy and function of the pelvic diaphragm and perineal body using a “string model”. Adv Physiol Educ. 2008; 32(2):169–70. [PubMed: 18539862]
40. Badylak SF, Lantz GC, Coffey A, Geddes LA. Small intestinal submucosa as a large diameter vascular graft in the dog. J Surg Res. 1989; 47(1):74–80. [PubMed: 2739401]
41. Brown B, Lindberg K, Reing J, Stolz DB, Badylak SF. The basement membrane component of biologic scaffolds derived from extracellular matrix. Tissue Eng. 2006; 12(3):519–26. [PubMed: 16579685]
42. Valentin JE, Stewart-Akers AM, Gilbert TW, Badylak SF. Macrophage participation in the degradation and remodeling of extracellular matrix scaffolds. Tissue Eng Part A. 2009; 15(7): 1687–94. [PubMed: 19125644]
43. Kamentsky L, Jones TR, Fraser A, Bray MA, Logan DJ, Madden KL, et al. Improved structure, function and compatibility for CellProfiler: modular high-throughput image analysis software. Bioinformatics. 2011; 27(8):1179–80. [PubMed: 21349861]
44. Lamprecht MR, Sabatini DM, Carpenter AE. CellProfiler: free, versatile software for automated biological image analysis. Biotechniques. 2007; 42(1):71–5. [PubMed: 17269487]
45. Butcher DT, Alliston T, Weaver VM. A tense situation: forcing tumour progression. Nat Rev Cancer. 2009; 9(2):108–22. [PubMed: 19165226]
46. Calve S, Odelberg SJ, Simon HG. A transitional extracellular matrix instructs cell behavior during muscle regeneration. Dev Biol. 2010; 344(1):259–71. [PubMed: 20478295]
47. Beattie AJ, Gilbert TW, Guyot JP, Yates AJ, Badylak SF. Chemoattraction of progenitor cells by remodeling extracellular matrix scaffolds. Tissue Eng Part A. 2009; 15(5):1119–25. [PubMed: 18837648]
48. Voytik-Harbin SL, Brightman AO, Kraine MR, Waisner B, Badylak SF. Identification of extractable growth factors from small intestinal submucosa. J Cell Biochem. 1997; 67(4):478–91. [PubMed: 9383707]
49. Zantop T, Gilbert TW, Yoder MC, Badylak SF. Extracellular matrix scaffolds are repopulated by bone marrow-derived cells in a mouse model of achilles tendon reconstruction. J Orthop Res. 2006; 24(6):1299–309. [PubMed: 16649228]
50. Agrawal V, Johnson SA, Reing J, Zhang L, Tottey S, Wang G, et al. Epimorphic regeneration approach to tissue replacement in adult mammals. Proc Natl Acad Sci USA. 2010; 107(8):3351–5. [PubMed: 19966310]

51. Tidball JG, Villalta SA. Regulatory interactions between muscle and the immune system during muscle regeneration. Am J Physiol Regul Integr Comp Physiol. 2010; 298(5):R1173–87. [PubMed: 20219869]

52. Martinez FO, Gordon S, Locati M, Mantovani A. Transcriptional profiling of the human monocyte-to-macrophage differentiation and polarization: new molecules and patterns of gene expression. J Immunol. 2006; 177(10):7303–11. [PubMed: 17082649]

53. Mantovani A, Sica A, Sozzani S, Allavena P, Vecchi A, Locati M. The chemokine system in diverse forms of macrophage activation and polarization. Trends Immunol. 2004; 25(12):677–86. [PubMed: 15530839]

54. Martinez FO, Sica A, Mantovani A, Locati M. Macrophage activation and polarization. Front Biosci. 2008; 13:453–61. [PubMed: 17981560]

55. Ruffell D, Mourkioti F, Gambardella A, Kirstetter P, Lopez RG, Rosenthal N, et al. A CREB-C/EBPbeta cascade induces M2 macrophage-specific gene expression and promotes muscle injury repair. Proc Natl Acad Sci U S A. 2009; 106(41):17475–80. [PubMed: 19805133]

56. Brown BN, Londono R, Tottey S, Zhang L, Kukla KA, Wolf MT, et al. Macrophage phenotype as a predictor of constructive remodeling following the implantation of biologically derived surgical mesh materials. Acta Biomater. 2012; 8(3):978–87. [PubMed: 22166681]

Appendix A. Supplementary data

Supplementary data related to this article can be found online at doi:10.1016/j.biomaterials.2012.04.017

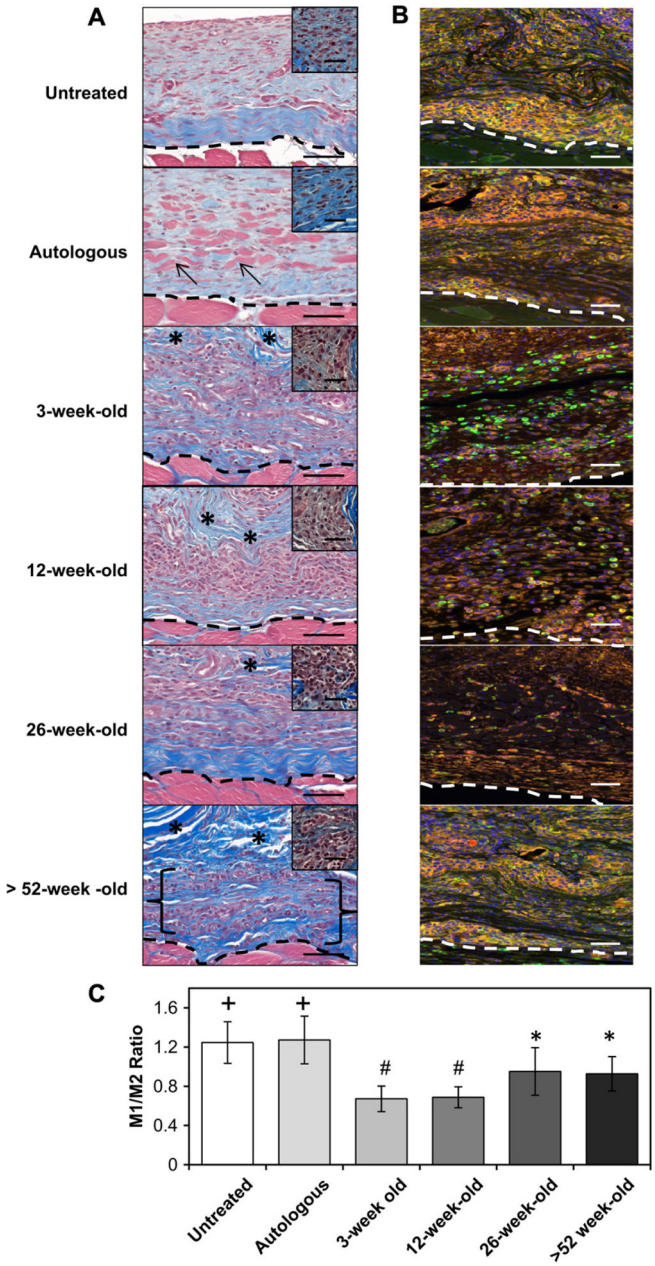

Fig. 1.

Host cellular response at the surgical site at 14 days post-surgery. The *in vivo* host response to untreated injury, autologous tissue graft, or scaffolds derived from differently aged source ECMs was assessed by histologic methods with Masson's Trichrome staining (A) and by the immunolabeling of macrophages (B & C). Necrotic islands of skeletal muscle could be identified within the implantation site of the autologous tissue graft (arrows). A mononuclear cell infiltrate (morphology depicted in high power inset) was identified throughout the 3,12, and 26-week-old scaffolds, while the >52-week-old scaffold was only partially infiltrated (bracket) (A). All treatment groups showed the presence of macrophages (CD68; Red). The untreated and autologous implant surgical sites displayed a predominant M1 macrophage (CCR7; Orange) phenotype (+, P <0.001 for both when compared to all other treatment groups). The >52 and 26-week-old implant sites were populated by a

balanced M1 to M2 macrophage (CD206; Green) ratio (#, $p < 0.004$ for both when compared to all other treatment groups). The 3 and 12-week-old scaffolds displayed a predominant M2 macrophage response (B & C; *, $p < 0.004$ for both when compared to all other treatment groups). Scale bars = 50 μm (inset scale bars = 20 μm), * = scaffold. Error bars = standard deviation. (For interpretation of the references to color in this figure legend, the reader is referred to the web version of this article.)

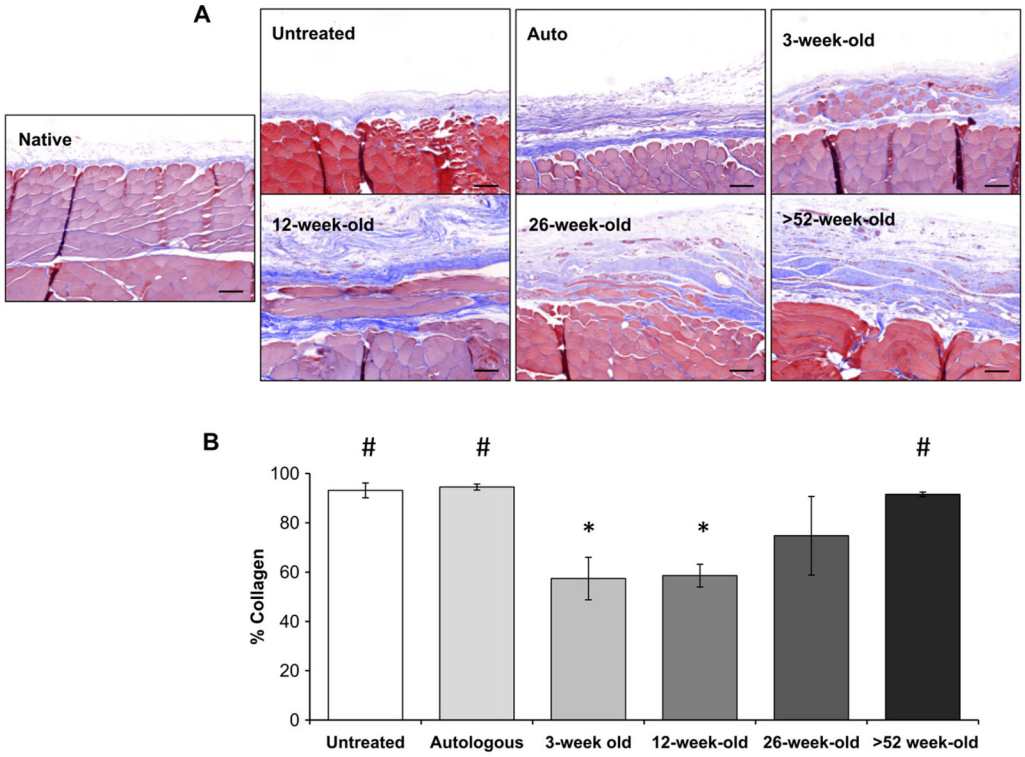

Fig. 2.

Remodeling outcomes at 180 days post-surgery. The remodeled tissue was assessed histologically with Masson's trichrome staining (A) and collagen content quantified (blue staining) using spectral unmixing (B). 3-week-old and 12-week-old scaffolds showed a constructive remodeling response after 180 days when compared to the untreated, autologous, or >52-week-old treated surgical sites as indicated by the formation of site appropriate skeletal muscle myofibers within the implant site (A & B). Collagen content showed 3 ($p < 0.007$) and 12-week-old ($p < 0.003$) scaffolds had significantly less collagenous tissue than the untreated, autologous, or >52-week-old treatment groups (B). Means with different symbols are significantly different. Scale bars = 50 μm. Error bars = standard deviation.

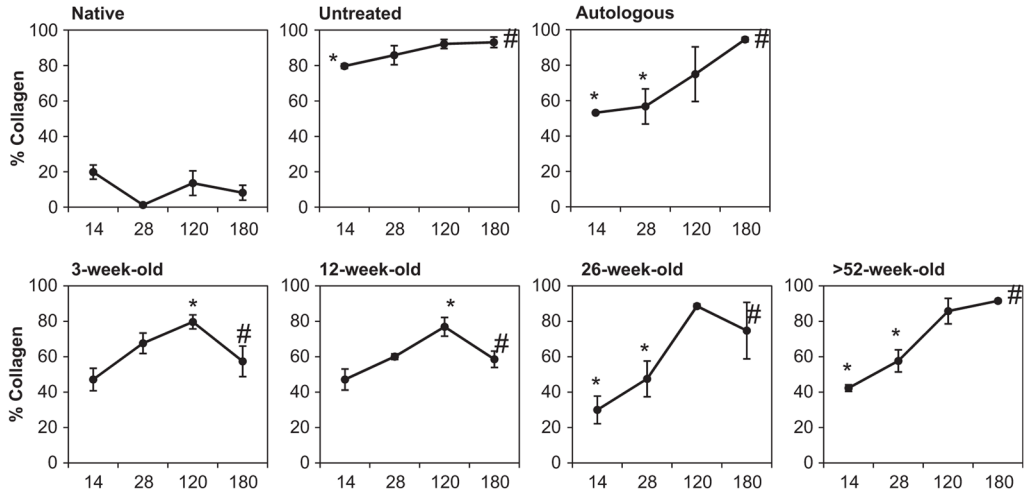

Fig. 3.

Connective tissue deposition within each surgical site over time. Quantification of Masson's trichrome, in terms of % collagen (blue staining), using spectral unmixing. Untreated defects as well as the autograft and sow aged scaffolds induced a steady increase in connective tissue deposition from 14 to 180 days post-surgery. Whereas, the feeder and neonate aged scaffolds were associated with a lower collagen presence more similar to that seen in native tissue. Means with different symbols are significantly different within each age group. Error bars = standard deviation.

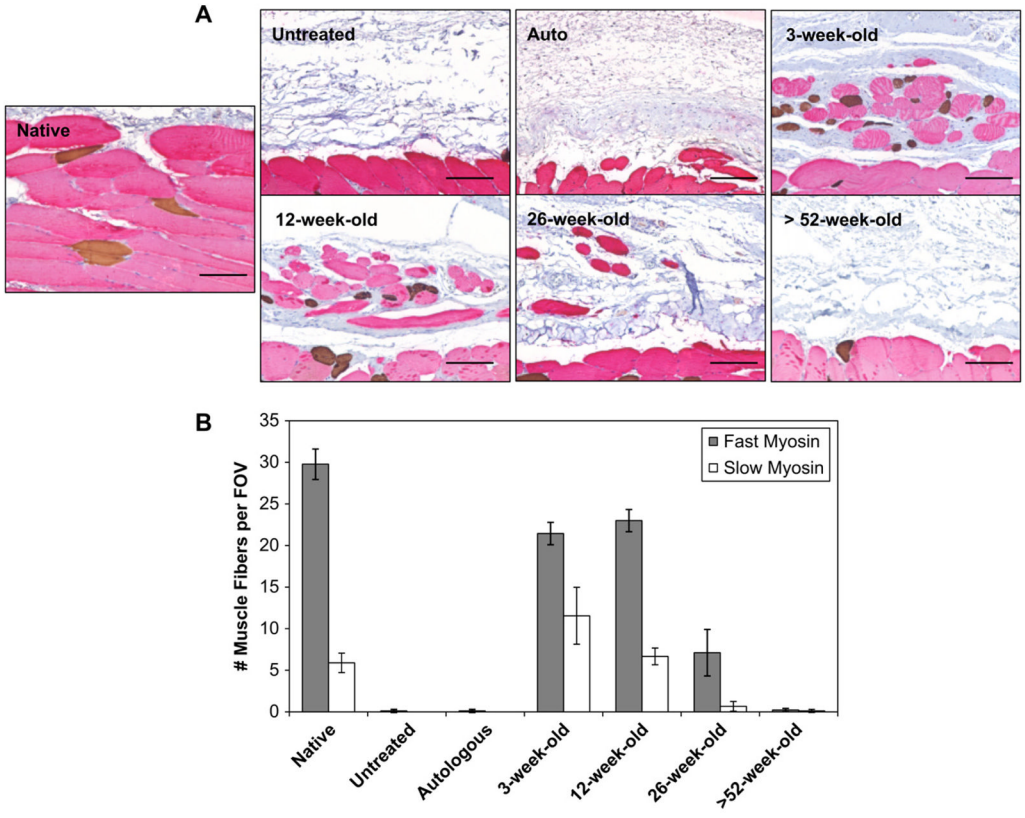

Fig. 4.

Distribution of slow and fast skeletal muscle fibers within the remodeled tissue at 180 days post-surgery. Tissue sections were double-labeled for anti-myosin slow (type I) skeletal muscle (brown stain) and anti-myosin fast (type II) skeletal muscle (red stain) to assess myofiber phenotype in the native and remodeled tissue (A). The native tissue showed that the slow muscle fibers were uniformly distributed between the fast muscle fibers. The remodeled 3 and 12-week-old scaffolds showed a similar distribution. 26-Week-old scaffolds showed predominantly fast muscle fibers, whereas the untreated defects, autograft, and >52-week-old scaffolds showed no signs of myofiber expression. Quantification of fast vs. slow muscle fibers per field of view (FOV) showed 3-week-old scaffolds displayed an increased number of slow muscle fibers when compared to all other surgical sites (B). Scale bars = 50 μm. Error bars = standard deviation.

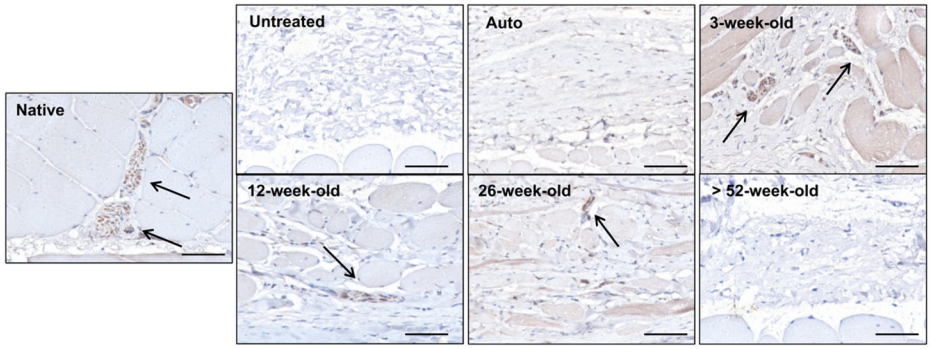

Fig. 5.

Innervation of remodeled tissue at 180 days post-surgery. Tissue sections were immunolabeled for anti-beta-III Tubulin (arrows; brown stain) to identify neurons in the native and remodeled tissue sections. Neurons were located adjacent to the myofiber bundles within the native tissue. Similar nerve structures were found around myofibers within the remodeled 26, 12, and 3-week-old scaffolds. The remodeled untreated defect site along with the >52-week-old scaffold and autograft treated sites showed no signs of innervation. Scale bars = 50 μm.

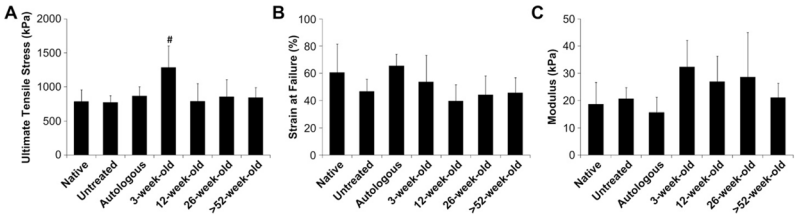

Fig. 6.

Mechanical properties of explanted surgical sites at 180 days post-surgery. Uniaxial tensile testing of explants (full thickness of the body wall including underlying and remodeled tissue) was used to characterize tissue mechanical properties for comparison to native tissue with respect to strength, distensibility, and stiffness. Body wall with remodeled 3-week-old aged SIS-ECM grafts withstood greater stress compared to native body wall and all other treatment groups (A). No differences were detected in strain at failure (B) or modulus (C) between native body wall and any other treatment group (#, $p < 0.05$). Error bars = standard deviation. Error bars = standard deviation.

Table 1

A summary of the pre-implantation properties of the differently aged ECM scaffolds. Adapted from Tottey et al., 2011 [38] with permission.

Age (Weeks)	Elastic modulus (MPa)	Stress (MPa)	Thickness (mm)	bFGF (ng/g dry weight material)	VEGF (pg/g dry weight material)	sGAG (μg/mg dry weight material)
3	0.8 ± 0.6	13.76 ± 12.70	14.00 ± 1.65	49.27 ± 1.70	510 ± 52	12.84 ± 0.09
12	1.9 ± 0.9	28.18 ± 13.05	23.15 ± 2.33	113.90 ± 0.36	810 ± 26	13.33 ± 0.33
26	2.0 ± 0.6	31.24 ± 9.93	24.75 ± 2.61	95.06 ± 0.86	825 ± 42	11.09 ± 0.36
>52	1.2 ± 0.7	22.20 ± 8.69	33.97 ± 2.16	77.93 ± 0.19	490 ± 10	10.06 ± 0.48

Table 2

Tissue assessment. All samples received Massons's trichrome and vasculature (CD31) staining with associated histologic assessment (×). Staining for macrophages was done at a time point consistent with a robust host macrophage response (14 days). Mechanical testing, along with staining for muscle fiber phenotype (myosin) and innervation (β-tubulin III), was included where trichrome staining confirmed the presence of skeletal muscle within the defect site (180 days).

Analysis	Harvest time point			
	14 days	28 days	120 days	180 days
Trichrome staining ($n = 3$)	×	×	×	×
CD31 staining ($n = 3$)	×	×	×	×
Macrophage staining ($n = 3$)	×	–	–	–
Fast/slow myosin staining ($n = 3$)	–	–	–	×
β-tubulin III staining ($n = 3$)	–	–	–	×
Mechanical testing ($n = 5$)	–	–	–	×